

1 Observations of the Lower Atmosphere From the 2021 WiscoDISCO 2 Campaign

3
4 Patricia A. Cleary¹, Gijis de Boer^{2,3,4}, Joseph P. Hupy⁵, Steven Borenstein⁴, Jonathan Hamilton^{2,3}, Ben
5 Kies¹, Dale Lawrence⁶, R. Bradley Pierce⁷, Joe Tirado¹, Aidan Voon¹, Timothy Wagner⁷

6
7 ¹ Department of Chemistry, University of Wisconsin Eau-Claire, Eau-Claire, WI, 54701, USA

8 ² Cooperative Institute for Research in Environmental Sciences, University of Colorado Boulder,
9 Boulder, CO, 80309, USA

10 ³ Physical Sciences Laboratory, National Oceanic and Atmospheric Administration, Boulder, CO,
11 80305, USA

12 ⁴ Integrated Remote and In Situ Sensing, University of Colorado Boulder, Boulder, CO, 80309, USA

13 ⁵ School of Aviation and Transportation Technology, Purdue University, West Lafayette, IN, 47907,
14 USA

15 ⁶ Research and Engineering Center for Unmanned Vehicles, University of Colorado Boulder, Boulder,
16 CO, 80309, USA

17 ⁷ Space Science and Engineering Center, University of Wisconsin Madison, Madison, WI, 53706, USA

18
19 *Correspondence to:* Patricia A. Cleary (clearypa@uwec.edu)

20 **Abstract.** The meso-scale meteorology of lake breezes along Lake Michigan impacts local observations
21 of high ozone events. Previous manned aircraft and UAS observations have demonstrated non-uniform
22 ozone concentrations within and above the marine layer over water and within shoreline environments.
23 During the 2021 Wisconsin's Dynamic Influence of Shoreline Circulations on Ozone (WiscoDISCO-21)
24 campaign, two UAS platforms, a fixed-wing (University of Colorado RAAVEN) and a multirotor (Purdue
25 University DJI M210), were used simultaneously to capture lake breeze during forecasted high ozone
26 events at Chiwaukee Prairie State Natural Area in southeastern Wisconsin from May 21-26, 2021. The
27 RAAVEN platform (data DOI: 10.5281/zenodo.5142491) measured temperature, humidity, and 3-D
28 winds during 2-hour flights following two separate flight patterns up to 3 times per day at altitudes
29 reaching 500 m above ground level. The M210 platform (data DOI: 10.5281/zenodo.5160346) measured
30 vertical profiles of temperature, humidity and ozone during 15-minute flights up to 6 times per day at
31 altitudes reaching 120 m above ground level (AGL) near to a WI-DNR ground monitoring station (AIRS
32 ID: 55-059-0019). This campaign was conducted in conjunction with the Enhanced Ozone Monitoring
33 plan from WI-DNR that included Doppler lidar wind profiler observations at the site (data
34 DOI:10.5281/zenodo.5213039).
35

36 **1. Introduction**

37 The WiscoDISCO-21 (Wisconsin's Dynamic Influence on Shoreline Circulations on Ozone) was
38 designed to capture lake breeze influence on the shoreline ozone observations and to interrogate the low-
39 altitude dimensionality of the marine layer as it moves on shore. The lake breeze is a mesoscale
40 phenomenon driven by differential air temperatures over land and water surfaces, which in spring and
41 early summer produces a solenoidal circulation in a baroclinic environment that manifests itself as
42 onshore flow during the day. A strong inversion develops as a shallow layer of maritime air is advected
43 onshore and displaces the warmer terrestrial air upward (Holton, 1992; Miller et al., 2003; Martin, 2006;
44 Wagner et al., 2022). These circulations can act as a transport mechanism of emissions on land to over
45 water at night and in early morning hours, then allowing those emissions to not mix when trapped in
46 cooler, temperature inverted air masses over water, eventually being driven back on land through a lake
47 breeze. The goals of the campaign were to: a) characterize lake breeze characteristics of near shore
48 circulation onset and vertical shape along the shoreline of Lake Michigan, b) capture the development or
49 movement of convergence zones/fine scale circulations within the lake-breeze frontal region from
50 offshore to onshore over time and c) monitor ozone gradients, characteristics of chemical circulation
51 patterns within marine-influenced inversions at the shoreline at low altitudes.

52 The influence of lake breeze on shoreline air quality along Lake Michigan (Keen and Lyons, 1978;
53 Lyons and Cole, 1976; Lyons and Olsson, 1973; Dye et al., 1995; Foley et al., 2011; Stanier et al., 2021)
54 and other Great Lakes (Hayden et al., 2011; Levy et al., 2010; Wentworth et al., 2015; Sills et al., 2011)
55 is well documented by campaigns incorporating ground (Lyons and Cole, 1976), ferry (Lennartson and
56 Schwartz, 2002; Cleary et al., 2015) and aircraft observations (Dye et al., 1995; Foley et al., 2011; Hayden
57 et al., 2011; Stanier et al., 2021). The shoreline communities of Lake Michigan have historically been in
58 non-attainment of federal ozone standards. Precursors to ozone production, volatile organic compounds,
59 (VOCs) and nitrogen oxides (NO_x), have emission sources along the Chicago urban corridor and ozone
60 production can be enhanced when those emissions are trapped in the marine layer over the lake and get
61 transported northward from Chicago (Vermeuel et al., 2019; Dye et al., 1995; Foley et al., 2011). The low
62 altitude features in ozone gradients over Lake Michigan have been observed in the recent 2017 Lake
63 Michigan Ozone Study field campaign (Stanier et al., 2021; Doak et al., 2021). Stanier et al. (2021)

64 describe observations for the highest measured ozone during the field campaign existing over water,
65 offshore from Milwaukee and in the altitude range of 30-100 m above lake level. Air quality models have
66 been shown to inadequately represent overwater ozone (Cleary et al., 2015; McNider et al., 2018; Qin et
67 al., 2019) and do not always capture the ozone gradients at the shoreline (Stanier et al., 2021; Abdi-
68 Oskouei et al., 2020). The shallow marine layer disruption when crossing a shoreline boundary during a
69 lake breeze is a unique environment to study the changes in vertical mixing and pollutant extent.

70

71 WiscoDISCO-21 featured round-based Doppler lidar observations and two Uncrewed Aircraft Systems
72 (UAS), including the University of Colorado RAAVEN fixed-wing UAS and Purdue University's DJI
73 M210 quadcopter. These platforms were deployed to enhance the level of detail and extend the domains
74 of ground-based measurements to manned aircraft observations with higher spatial resolution and
75 sustained lower-altitude flight. UAS are well suited to make observations of a shoreline environment
76 impacted by a shallow marine layer, where vertical mixing and pollutant transport are key to
77 understanding pollution events at the surface. UAS have been used in riverine environments to highlight
78 pollutant transport and nighttime boundary layer dynamics (Guimaras et al., 2020). During the Ozone
79 Water-Land Environmental Transition Study (OWLETs), UAS, ozone sondes and lidar observations were
80 used to observe ozone titration events above the Chesapeake Bay shipping channel (Gronoff et al., 2019).
81 Horel et al., (Horel et al., 2016) describe the use of distributed ground sensors, tethered sondes and UAS
82 to better understand the meteorological and pollutant transport factors surrounding poor air quality in the
83 Salt Lake Valley. The incorporation of multi-hole probes into fixed-wing UAS has allowed for
84 observations of 3-D winds (Elston et al., 2015) and turbulent fluxes (Wildmann et al., 2014). The
85 RAAVEN platform leveraged in WiscoDISCO-21 has recently been used to study the lower atmosphere
86 across a variety of environmental regimes. This includes nearly a month of flight operations to investigate
87 the thermodynamic and kinematic structure of trade winds over the tropical Atlantic Ocean, (de Boer et
88 al. (2021a) as well as deployments to the US Midwest to make measurements of supercell thunderstorms
89 (Frew et al., 2020). The measurement accuracy of the RAAVEN's instrumentation was recently evaluated
90 at the US Department of Energy's Atmospheric Radiation Measurement (ARM) program's Southern
91 Great Plains facility (see de Boer et al. (2021b) for details).

92

93 Such high-resolution UAS observations are well-suited for documenting and characterizing the
94 dimensions of the lake breeze phenomenon and corresponding pollutant transport. A combination of UAS
95 and lidar can provide overlapping domains of observations that scale up to the planetary boundary layer,
96 with UAS providing detailed insight into nonuniformities in meteorological observations along the Lake
97 Michigan shoreline. UAS observations are particularly complementary to Doppler lidar observations, as
98 such observations are subject to near-field issues that prevent them from making observations at very low
99 altitudes. Given that the UAS readily operate between the surface and 100 m, these platforms can fill in
100 this gap and provide detailed insight into thermodynamic, kinematic and chemical properties of this layer.
101 These observations have higher vertical and temporal resolution than many chemical models which can
102 provide insight into model resolution issues at the lake-land interface (Wagner et al., 2021). The
103 WiscoDISCO-21 field campaign was conducted in conjunction with the Enhanced Ozone Monitoring
104 initiative from the Wi-DNR who housed added instrumentation for NO, NO_x (NO_x = NO + NO₂) NO_y
105 (NO_y = sum of all reactive nitrogen species), , VOC canisters and PANDORA instrumentation at the
106 Chiwaukee Prairie air monitoring station. The NO, NO_x and VOC measurements can give some indication
107 of the availability of precursors for ozone production and NO_y measurements along with some specific
108 VOCs can indicate something about the past ozone production history of an air parcel. The WiDNR has
109 provided a portal for access to data from these sensors through their web portal ([https://wi-
110 dnr.widencollective.com/portals/iwvftorq/AirMonitoringData](https://wi-dnr.widencollective.com/portals/iwvftorq/AirMonitoringData)).

111 These data sets can be used in a variety of ways to better understand the meteorology and
112 pollution episodes at the Lake Michigan shoreline. The Lidar WindPRO data and RAAVEN data
113 provide complete coverage of the atmospheric dynamics of the marine layer such that it can be
114 characterized and modeled (Wagner et al., 2022; Jozef et al., submitted); Those characterizations could
115 be used to test the fidelity of operational meteorological models (such as HRRR) in modeling the stable
116 boundary layer height. The data sets can also be used to test models for the roughness parameterizations
117 in a shoreline environment using overwater and overland turbulences. The combination of ozone data
118 with the meteorological data can be used to constrain air quality models for the chosen mixing volume
119 for chemical processing in the atmosphere, using the FOAM model (Vermeuel et al., 2019) or testing

120 vertical grid-scale sizing of nested high resolution models for their ability to reproduce the gradients in
121 ozone as measured using UAS (Abdi-Oskouei et al., 2020). The lake breeze phenomenon is similar to
122 bay breeze and sea breeze circulations that complicate modeling efforts in other shoreline locations
123 impacted by poor air quality (Caicedo et al., 2021; Geddes et al., 2021) and model fidelity is crucial to
124 the development of appropriate emissions controls in these environments.

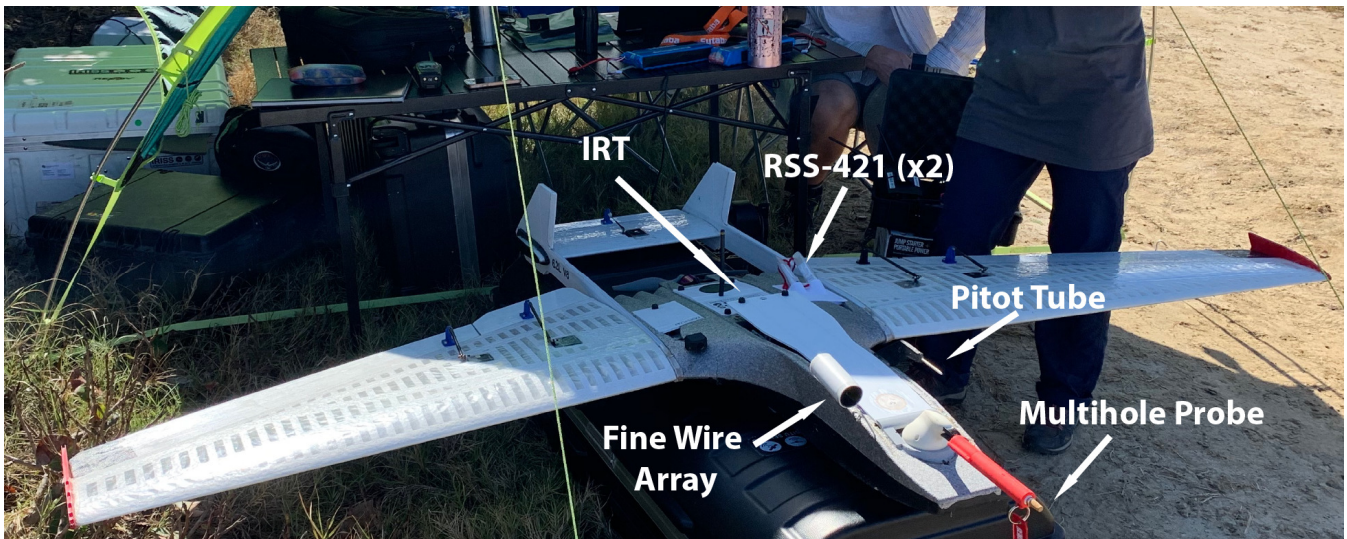
125 **2. Description of Instrumentation and Vehicles**

126 **2.1 University of Colorado RAAVEN UAS**

127 The RAAVEN UAS (Fig. 1) is a fixed-wing UAS with a wingspan of 2.3 m that has been operated by the
128 University of Colorado Boulder since 2019. The RAAVEN's airframe is based on a custom-manufactured
129 model from RiteWing RC. The airframe has been updated to meet the needs of atmospheric science
130 missions spanning a variety of environments. The RAAVEN leverages the PixHawk2 autopilot system
131 and employs an 8S 21000 mAh Lithium Ion (Li-Ion) battery pack to offer flight times around 2.5 hours,
132 depending on conditions and executed flight patterns. Specific modifications to the airframe include the
133 integration of a tail boom to enhance longitudinal stability and improve the platform's performance. The
134 aircraft has a top airspeed of approximately 130 km hr^{-1} , though operations during WiscoDISCO-21 were
135 almost exclusively conducted in the $60\text{-}70 \text{ km hr}^{-1}$ range.



136



137
 138
 139
 140

Figure 1: The University of Colorado RAAVEN being prepared for launch during WiscoDISCO21 (top), and a close up of the RAAVEN sensing systems (bottom).

141

142 For the WiscoDISCO-21 campaign, the RAAVEN was equipped with an instrument suite derived from
 143 the *miniFlux* payload co-developed by the National Oceanic and Atmospheric Administration (NOAA),
 144 the Cooperative Institute for Research in Environmental Sciences (CIRES) and Integrated Remote and In
 145 Situ Sensing (IRISS) at the University of Colorado. In this configuration, the aircraft was set up to
 146 measure atmospheric and surface properties to support evaluation of thermodynamic state, kinematic
 147 state, and turbulent fluxes of heat and momentum. This involves a suite of core instrumentation (see Fig.
 148 3), including a multihole pressure probe (MHP) from Black Swift Technologies, LLC (BST), a pair of
 149 RSS421 PTH (pressure, temperature, humidity) sensors from Vaisala, Inc., a custom finewire array,
 150 developed and manufactured at the University of Colorado Boulder, a pair of Melexis MLX90614 IR
 151 thermometers, and a VectorNav VN-300 inertial navigation system (INS). This sensor suite is logged
 152 using a custom- designed FlexLogger data logging system.

153

154 The Vaisala RSS421 sensors are identical to those used in the Vaisala RD41 dropsonde, and very similar
 155 to the Vaisala RS41 radiosonde. This unit employs a linear resistive platinum temperature sensor with a
 156 resolution of 0.01 °C, repeatability of 0.1 °C and a response time (as measured within the RS41

157 radiosonde) of 0.5 s at 1000 hPa when moving at 6 m s⁻¹. For relative humidity (RH), the RSS421 includes
158 a thin-film capacitor with a resolution of 0.1% RH and a repeatability of 2% RH, with a temperature-
159 dependent response time of better than 0.3 s at 20 °C (again, as measured within the RS41, with 6 m s⁻¹
160 airflow at 1000 hPa). Finally, the pressure sensor is capacitive with a silicon diaphragm, having a
161 resolution of 0.01 hPa and a repeatability of 0.4 hPa. For WiscoDISCO-21, a pair of these sensor modules
162 was mounted to the top of the RAAVEN's fuselage, between the nose and the tail of the aircraft on the
163 port side. The sensor mounting angles were offset to ensure that the two sensors would have different
164 amounts of solar exposure as the aircraft maneuvers through the atmosphere and to allow for the detection
165 of solar heating effects since no shading is used. Additional information on atmospheric thermodynamic
166 state is available from an E+E EE-03 sensor that is integrated into the BST MHP and from a Sensiron
167 SHT-85 sensor that is integrated in the custom finewire array. The EE-03 has a temperature accuracy (at
168 20 °C) of 0.3 °C, while the humidity accuracy is stated to be 3% RH at 21 °C. The SHT-85 has a stated
169 temperature accuracy of 0.1 °C (from 20-50 °C) and a repeatability of 0.08 C, while the humidity sensor
170 has a stated accuracy of 1.5% RH and a repeatability of 0.15 % RH. Both the EE03 and the SHT-85
171 sensors have slower response times than the RSS421 sensor described above and are typically not used
172 for scientific purposes unless there is a complete failure of the RSS421.

173

174 In addition to the SHT-85 sensor, the finewire array consists of two 5 µm diameter platinum wires
175 extending over a 2 mm length, suspended in the free stream by supporting prongs. One wire is operated
176 as a hotwire anemometer, with approximately 100 °C overheating compared to the ambient environmental
177 temperature. The other wire is operated as a coldwire thermometer, with approximately 1 °C overheating
178 relative to the surrounding environment. The wires have thermal time constants of 0.5 ms in a 15 m s⁻¹
179 airflow regime and support a sampling frequency of up to 800Hz to support measurement of turbulent
180 fluctuations in velocity and temperature. An electronics module converts resistance change in the wires
181 due to velocity or temperature variability to amplified voltages. For WiscoDISCO-21, the finewire was
182 logged at 250 Hz by the FlexLogger, which is equivalent to a 7.2 cm minimum length scale at the
183 RAAVEN's typical cruise airspeed of 18 m s. Time series of these recorded data are processed during
184 post-flight analysis to transform the voltages recorded by the fine wire module to velocity and

185 temperature. Additionally, these measured quantities can be fit to inertial sub-range turbulence models to
186 wavenumber spectra over suitable time intervals, producing turbulence intensity parameters epsilon
187 (kinetic energy dissipation rate) and CT^2 (temperature structure constant). The resolution (noise floor) of
188 these parameterizations is $2.0 \times 10^{-7} \text{W kg}^{-1}$ for epsilon and $4.5 \times 10 \text{ K m}$ for CT^2 . Resolution of the raw time
189 series are $8.3 \times 10 \text{ m s}$ for the hotwire and $1.3 \times 10 \text{ K}$ for the coldwire.

190

191 In addition to the EE-03 PTH measurements, the BST 5-hole probe supports measurement of airspeed,
192 angle of attack (α) and sideslip angle (β). These measurements are combined with the GPS-based ground
193 velocities and aircraft attitude from the VectorNav VN-300 to derive the three-components of the inertial
194 wind (u, v, w), as discussed in section 4. The VN-300 can be configured in a dual-Global Navigation
195 Satellite System (GNSS) mode, under which the relative positions of two GNSS antennae are used to
196 calculate the platform yaw. However, this setting was not used during the WiscoDISCO-21 deployment.
197 Under dynamic conditions, the system has a stated accuracy of 0.3 degrees in GPS- Compass heading,
198 0.1 degrees in pitch and roll, 2.5 m horizontal position accuracy, 2.5 m vertical position accuracy when
199 integrating information from the barometric pressure sensor, and 0.05 m s^{-1} accuracy in inertial velocity.
200 Input from the system's gyroscope, accelerometer, GNSS receiver, magnetometer and pressure sensor are
201 filtered through an extended Kalman Filter (EKF) to produce a navigation solution. VN-300 data were
202 logged at 50 Hz resolution during WiscoDISCO-21.

203

204 Finally, RAAVEN deploys two Melexis MLX90614 IR thermometers: one looking up from the top of
205 the aircraft and one looking down towards the surface in level flight. These sensors are factory calibrated
206 to work in operational temperatures between -40 and 125 C, and to measure target brightness temperatures
207 between -70 and 380 °C. They have a high accuracy (0.5 °C) and a measurement resolution of 0.02 °C.
208 The RAAVEN-mounted MLX90614s are not stabilized to maintain a vertical orientation, meaning that
209 the observed target is perpendicular to the reference frame of the aircraft. This requires some care when
210 interpreting measurement from time periods when the aircraft is conducting pitch or rolling maneuvers.
211 For WiscoDISCO-21, we leveraged the "T" version of this sensor which has a 5-degree field of view.
212 These sensors have a broad passband range of 5-14 μm , meaning that while it covers the infrared

213 atmospheric window, it is also subject to radiation emitted by water vapor and other radiatively active
214 gases, meaning that a significant depth of atmosphere between the aircraft and a given target (e.g., cloud;
215 surface), atmospheric gases influence the temperature reading. Despite this range spanning the 9.6 μm O_3
216 band, the relative proximity of the sensor to targets of interest (e.g. surface, clouds) means that this overlap
217 is not expected to significantly influence the readings, due to the integrated path length being relatively
218 small. Therefore, if absolute accuracy of brightness temperature is important, the sensor should be
219 operated in close proximity to a target of interest. However, relative contributions from different surface
220 types or atmospheric conditions can still be easily distinguished despite a lack of absolute calibration for
221 extended distance sensing. Such gradient detection can be useful for detecting surface inhomogeneities,
222 or for understanding whether the aircraft is operating under cloud or clear sky.

223

224 **2.2 M210 UAS**

225 The DJI M210 quad copter was equipped with a 3-D printed top-mounted bracket for holding a 2B
226 Technologies Personal Ozone Monitor (POM) and an Internet Systems iMET-XQ2 meteorology sensor
227 (Fig. 2). The copter had a ~15 minute flight time with the on-board sensors without a camera. The POM
228 measures ambient ozone using UV absorption and active humidity subtraction by measuring a whole air
229 sample and an ozone scrubbed sample in a 10-s duty cycle. The POM records data to its internal data
230 storage at 10 s interval with a log number and time stamp along with GPS coordinates and instrumentation
231 metrics (optical cell pressure and temperature). The iMET system records temperature, humidity, and
232 pressure along with GPS coordinates and a time stamp to internal data storage. Each instrument (the POM
233 and iMET) had individual data logging systems and separate power supplies. Both the POM and the iMET
234 had GPS capabilities with the POM logging inconsistently and the iMET logging GPS more consistently.
235 Each instrument and the UAS flight recorder logged time stamps. The iMET recorded observations of
236 temperature, relative humidity, humidity temperature and pressure at a frequency of 10 Hz. The POM
237 recorded ozone observations at a frequency of 0.1 Hz. The POM, iMET and M210 time-stamps drifted
238 up to 60 seconds from the other logged data. The flight log recorded the M210 positioning (altitude,

239 latitude, longitude) at 100 Hz. The M210 flight logs, iMET data and POM data were each downloaded
240 separately after each series of flights.



241
242
243
244 **Figure 2:** DJI M210 multirotor UAS with bracket-mounted POM and iMET

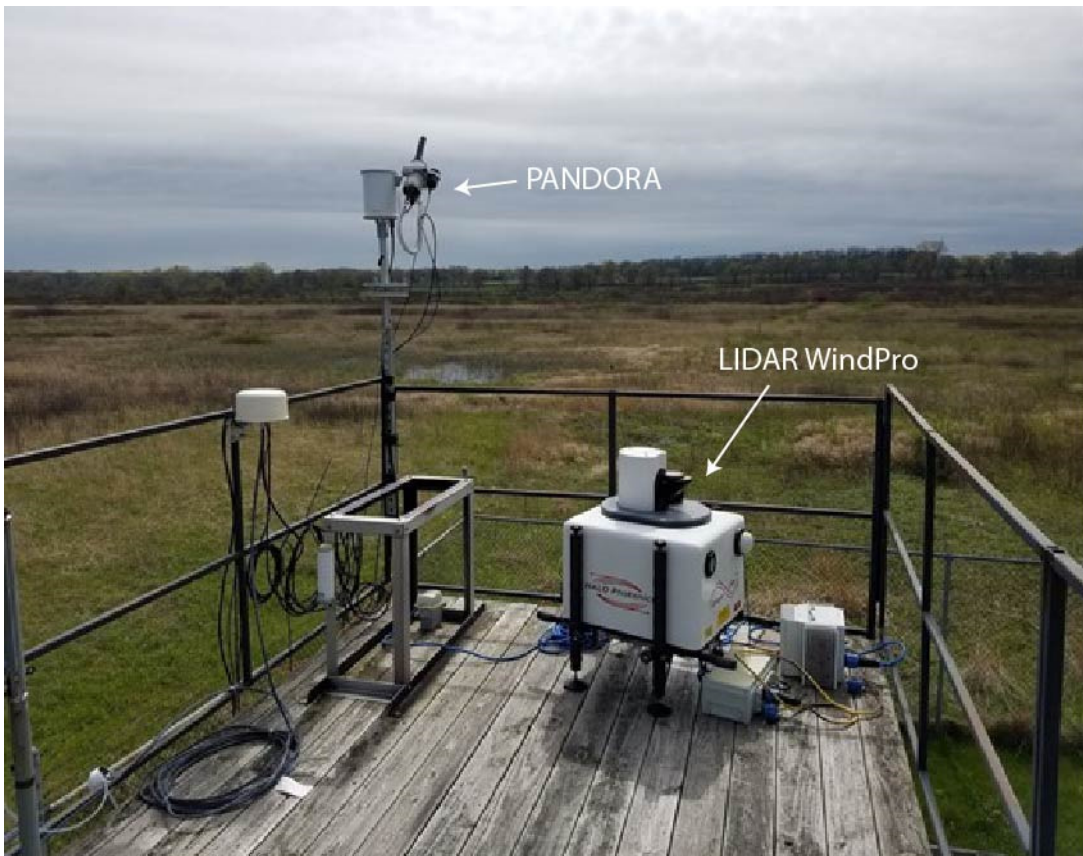
245

246 **2.3 Chiwaukee Lidar System**

247 A Halo Photonics Stream Line XR Doppler lidar (Pearson et al. 2009) was deployed on the roof of the
248 Chiwaukee Prairie air monitoring station (Fig. 3), approximately 3 m AGL. This is the same system that
249 is regularly deployed as part of the Space Science and Engineering Center (SSEC) Portable Atmospheric
250 Research Center, SPARC, (Wagner et al., 2019). The Doppler lidar actively emits pulses of near-infrared
251 radiation at a wavelength of 1.5 μm . This wavelength is long enough that molecular scattering causes
252 little attenuation of the signal, but it is short enough that it is sensitive to aerosols that are suspended
253 within the planetary boundary layer.

254

255 The Doppler lidar uses velocity-azimuth display (VAD) scans of the Doppler lidar to retrieve profiles of
256 wind speed and direction. In VAD, an instrument capable of measuring along-beam velocity (like a
257 Doppler radar or lidar) stares at multiple azimuths at a non-zenith elevation angle over a short period of
258 time, and then reconstructs the profile of winds above the lidar by assessing how the along-beam velocity
259 changes as a function of azimuth and range. For WiscoDISCO-21, the VAD scans were configured with
260 six azimuthal stares per profile (at azimuths of 0 $^\circ$, 60 $^\circ$, 120 $^\circ$, and so on) with an elevation angle of 70 $^\circ$.
261 Range gates were 18 m. VAD scans were conducted every 4 min and each VAD took approximately 45
262 s to complete. Between VADs, the lidar reverted to vertical stares in order to capture profiles of
263 backscatter and vertical velocity. Since the lidar depends on the presence of scatterers to have a detectable
264 signal return, the depth of the retrieved wind profiles varied significantly throughout the experiment from
265 as shallow as 200 m to as deep as 2 km.



266
267
268
269
270

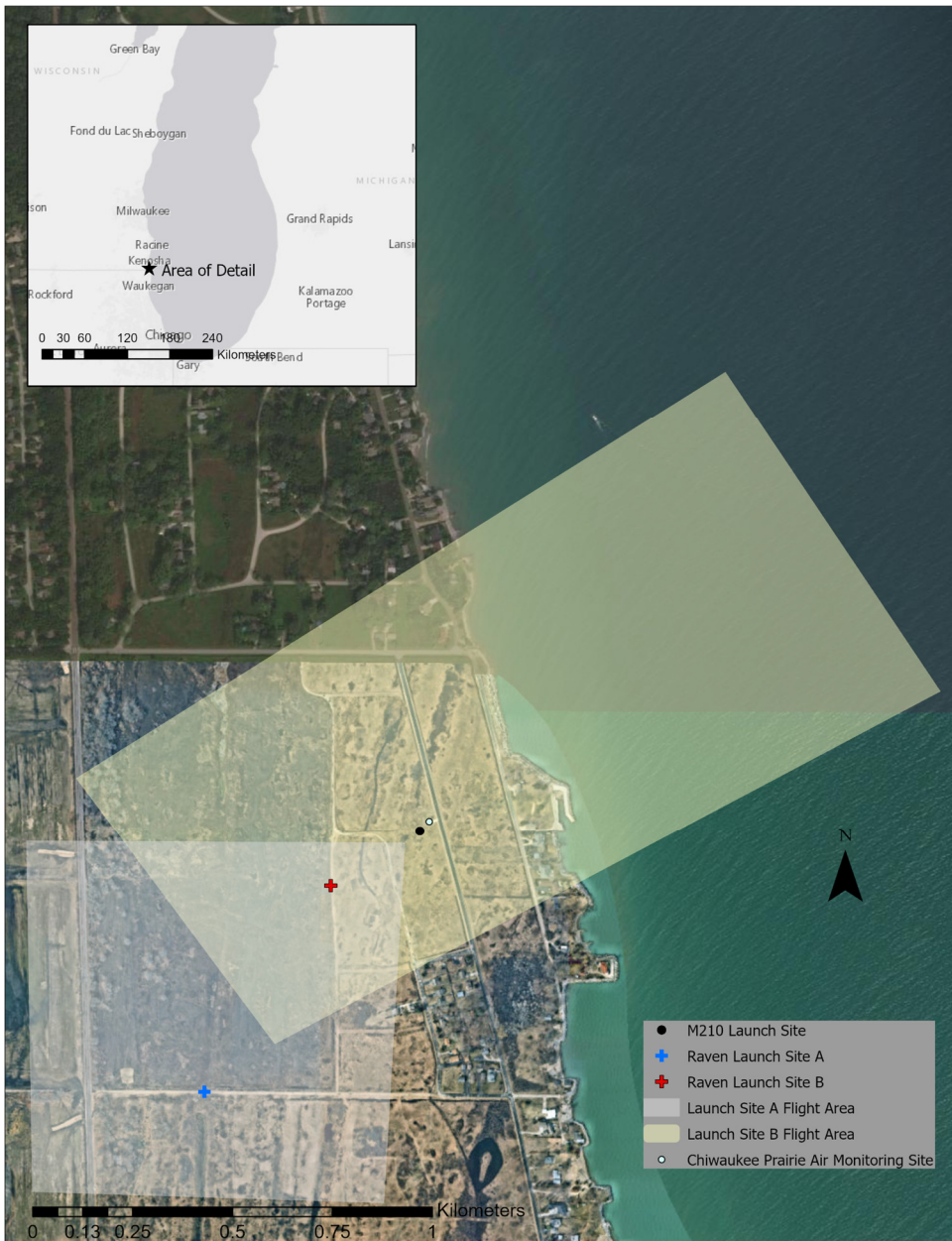
Figure 3: Roof of the Chiwaukee Prairie air monitoring system, showing the PANDORA (upper left) and Doppler lidar (right-center). The wooden floor pictured here is approximately 3 m above ground level.

271

272 **3. Description of measurement location, deployment strategies and sampling**

273 The Chiwaukee Prairie State Natural Area is a 485-acre shoreline prairie managed by the Wisconsin
274 Department of Natural Resources (WiDNR) located along the shoreline of Lake Michigan and adjacent
275 to the Wisconsin/Illinois border. The WiDNR operates an air monitoring station (Airs ID 55-059-0019)
276 for Kenosha County within this area, located at 11838 First Court in Pleasant Prairie, WI. This location
277 was chosen due to its suitability for UAS flight operations and the regular influence of lake breeze
278 circulations at the site. As a result of these lake breezes, the WiDNR's Chiwaukee Prairie Monitor
279 regularly observes some of the highest ozone concentrations in the state (Stanier et al., 2021) with a 2015-

280 2017 design value of 78 ppb (Cleary et al., 2022), where the federal ozone standard is 70 ppb for an 8-
281 hour average. Land use in the region is mixed suburban housing and farming, with two marinas directly
282 south of the research site. Chiwaukee Prairie has trail access along Al Kemper Trail and 122nd Street that
283 is isolated from automobile, bicycle and most pedestrian traffic. The M210 flights were conducted near
284 the WiDNR Air Monitoring site (Latitude: 42.5045, Longitude: -87.8095) and the RAAVEN flight
285 operations were conducted on Al Kemper Trail or 122nd St to provide ample room for take-off and
286 landing (Fig. 4).
287



288

289 **Figure 4:** Research site map including Chiwaukee Prairie air monitor and locations for launch sites for
 290 M210 and RAAVEN. Map created using Esri ArcPro version 2.52 using ArcPro basemap imagery.
 291

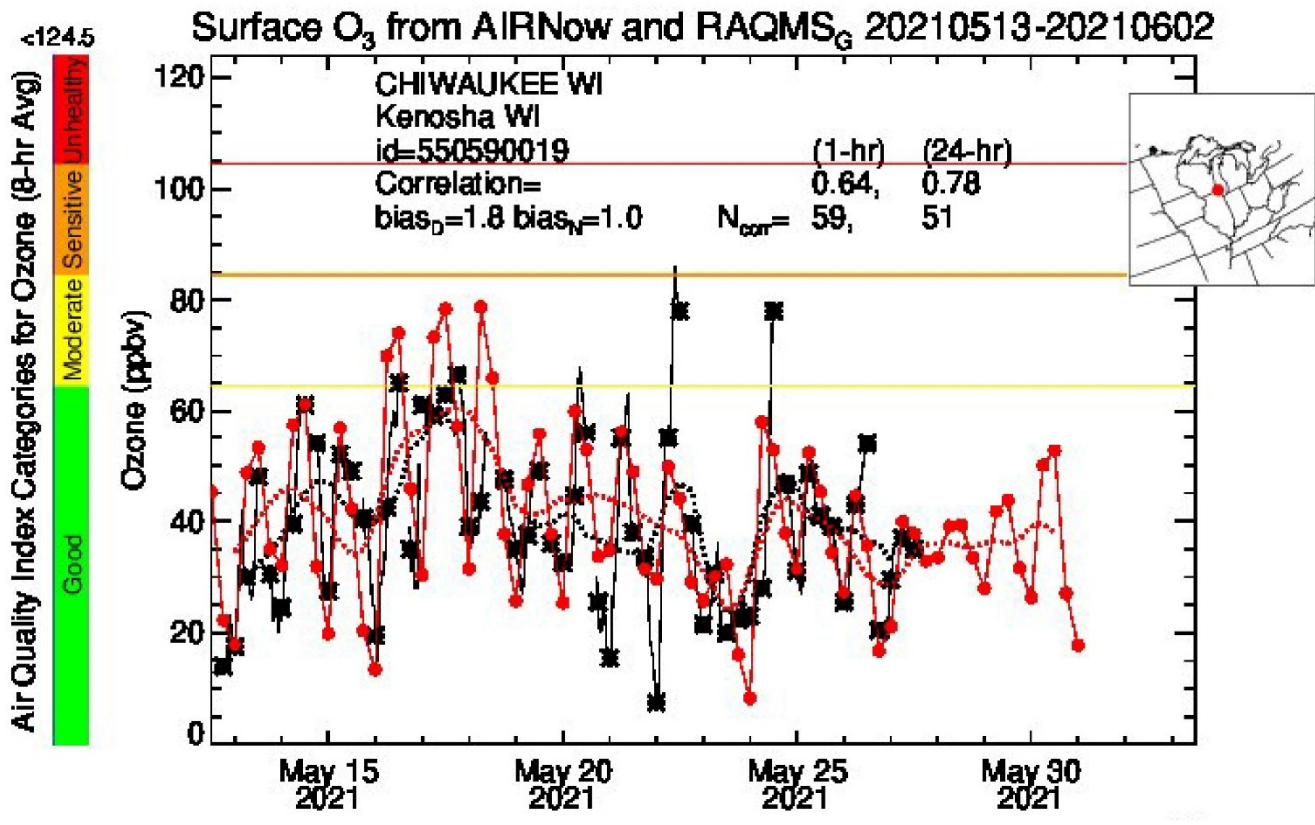
292

293 The primary goal for the field campaign was to capture elevated ozone concentration events resulting
 294 from lake breeze circulations at the site. The deployment strategy for selecting a time window for field

295 operations was dictated by ozone and meteorological forecasts that predicted light southerly winds for an
296 extended period that would both a) increase the likelihood of onshore lake breeze flow from weaker
297 southerly winds and b) drive pollutant transport from the Chicago metro area to the site.

298

299 Forecasts from both the WiDNR and Realtime Air Quality Modeling System (RAQMS) were
300 used to select an ideal deployment period. The dates of May 21-26, 2021 were chosen as meeting those
301 requirements. The selection of the time period for the campaign was dictated by capturing a
302 combination of lake breeze and ozone events. An acceptable window for operations from late May 23
303 through mid-June was targeted because of the higher frequency of high ozone and lake breeze events
304 occurring in this region during late spring/ early summer (see Cleary 2022, SI for a list of high ozone
305 events for the years 2013-2019 at Chiwaukee Prairie). Once the operations window was approaching,
306 the team used the RAQMS forecast model (Fig. 5) and consulted with the Wisconsin Department of
307 Natural Resources (WiDNR) Air Quality Division’s meteorologist to decide on a “go time” to initiate
308 deployment from all collaboration partners for an 8-day campaign. The go time required evidence that
309 synoptic flow would have a southerly component for a few days (normally brought about by a high-
310 pressure system over the Ohio River Valley) with limited precipitation events. Flights were canceled
311 during days in which high ozone or southerly/southeasterly lake breeze were not expected (Table 1).



312

313 **Figure 5:** 8-hour ozone concentrations from RAQMS forecast (red) and observations (black) for May 13-
 314 26, 2021 at Chiwaukee Prairie.

315

316 **Table 1:** UAS flight days and conditions for the WiscoDISCO-21 field campaign. Flight Pattern A and
 317 B are depicted in Figure 6 A.

318

Date (2021)	M210 (time UTC)	University of Colorado RAAVEN (Time UTC and flight pattern)	Weather and Air Quality Conditions
Friday, May 21	F1 (15:35-15:44) F2 (16:38-16:47) F3 (19:08-19:21) F4 (19:46-19:59)	F1 (15:01-16:54) Pattern A F2 (18:36-20:40) Pattern A	SW wind, Temps > 25 °C, small shift in winds to colder from SSE

Saturday, May 22	F1 (14:22-14:35) F2 (15:18-15:31) F3 (17:27-17:41) F4 (18:26-18:41) F5 (20:09-20:22) F6 (20:59-21:14)	F1 (13:52-15:55) Pattern A F2 (17:00-19:03) Pattern A F3 (19:30-21:38) Pattern A	W wind in AM, Temps > 25 °C, consistent shift in winds to colder from SSE.
Sunday, May 23	no flights	no flights	W to NE winds, dropping temperatures, AM showers, PM showers
Monday, May 24	F1 (15:08-15:23) F2 (16:01-16:16) F3 (18:14-18:29) F4 (19:12-19:27) F5 (21:09-21:19) F6 (22:04-22:19)	F1 (14:24-16:30) Pattern B F2 (17:41-19:50) Pattern B F3 (20:42-22:51) Pattern B	S winds, lake breeze, high ozone event (> 70 ppb).
Tuesday, May 25	F1 (14:00-14:15) F2 (14:49-15:04)	F1 (13:39-15:42) Pattern B	SW winds, slight lake breeze in the morning, overtaken by westerlies
Wednesday, May 26	F1 (13:43-13:58) F2 (14:37-14:52) F3 (16:47-17:02) F4 (17:47-18:01) F5 (19:51-20:06) F6 (20:48-21:01)	F1 (13:27-15:24) Pattern B F2 (16:31-18:20) Pattern B F3 (19:30-21:22) Pattern B	W wind, steady all day, sunny. After all flights, lake breeze came in from NE

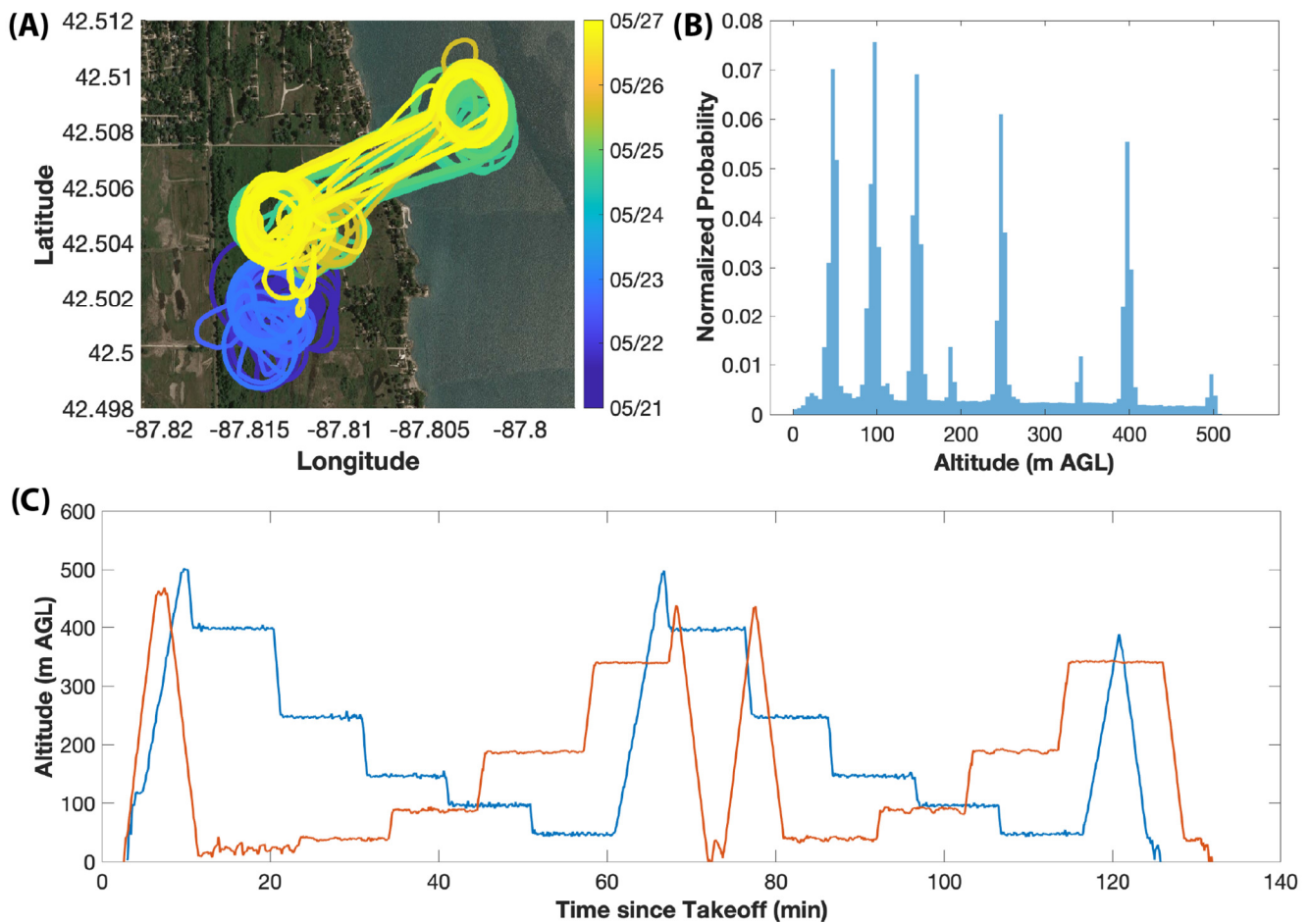
319
320
321

322 Flights were conducted in the time window 08:00-17:00 local time, CDT (13:00-22:00 UTC) (Table 1).
323 The RAAVEN platform features 2-hour flight times and was deployed to complete up to 3 flights per
324 day. The M210 flew slow ascents to 120 m AGL with an approximate 15-minute flight time, completing
325 up to 6 flights per day and the sampling pattern was designated to achieve maximum overlap with the
326 RAAVEN flight times by conducting two flights per RAAVEN flight.

327

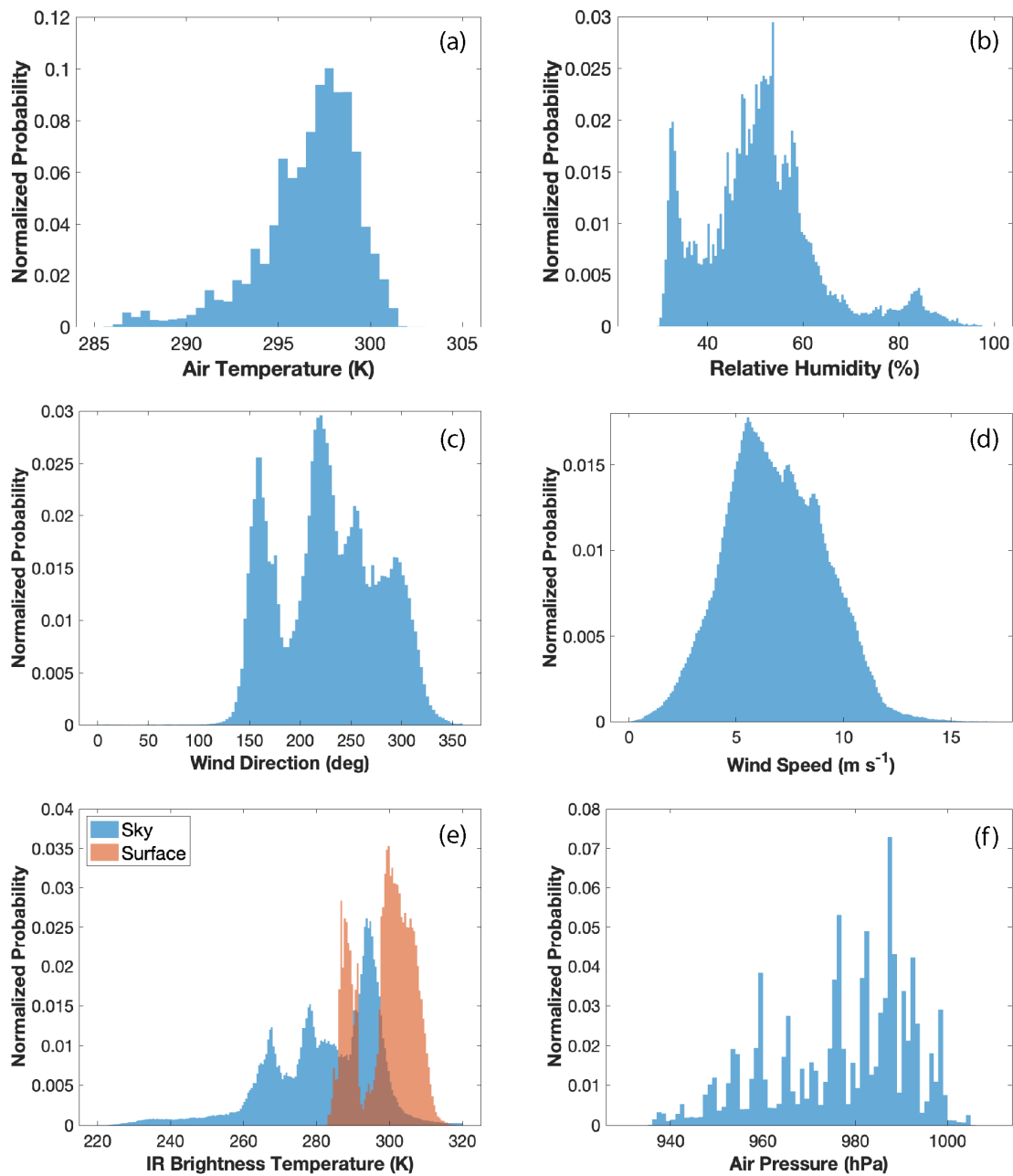
328

329 During WiscoDISCO-21, the RAAVEN completed 12 flights, totaling 25.4 flight hours, operating under
330 a Certificate of Authorization (COA) from the US Federal Aviation Administration (FAA) to allow flights
331 up to 518 m AGL. Fig. 6a shows a map of the RAAVEN flights, while figure 2b includes a histogram of
332 the altitudes covered by these flights. Flights were designed to follow two distinct flight patterns A and
333 B to capture over-prairie profiles using a circular pattern with holding at altitudes 400, 250, 150, 100 and
334 50 m AGL and over-water/over-prairie profiles using an extended racetrack pattern that traversed the
335 shoreline, with holding altitudes at 400, 250, 150, 100 and 50 m AGL (see Figure 6c for the two flight
336 patterns). Figure 7 shows histograms of the measurements obtained by the RAAVEN over the length of
337 the campaign, including temperature, relative humidity, wind speed, wind direction, air pressure, and
338 surface and sky brightness temperature.



339

340 **Figure 6:** A map showing the flight tracks for the RAAVEN with blue showing flight pattern A and
341 yellow or green showing flight pattern B (a), a histogram of altitudes sampled by the RAAVEN (b), and
342 example time-height plots of the two types of RAAVEN flights (c). The “normalized probability”
343 presented for a given bin is the number of elements in a given bin divided by the total number of elements
344 in the input data, so that the integral of the histogram equals one. Background maps are © GoogleMaps
345 2021, downloaded through their API.



346

347

348

349

350

Figure 7: Histograms of (a-f) temperature, relative humidity, wind direction, wind speed, IR brightness temperatures, and air pressure, as measured by the RAAVEN during WiscoDISCO-21. As in figure 6, the “normalized probability” presented for a given bin is the number of elements in a given bin divided by the total number of elements in the input data, so that the integral of the histogram equals one.

351 4. Data processing and quality control

352 4.1 University of Colorado RAAVEN UAS

353 Data collected by the different sensors carried by the RAAVEN during WiscoDISCO-21 were logged at
354 a variety of different logging rates. The finewire system was logged at 250 Hz, the fastest rate of all of
355 the sensors. The BST MHP was logged at 100 Hz, the VectorNav VN-300 at 50 Hz, the Melexis IR
356 sensors and variables related to finewire status were logged at 20 Hz, while data collected from the
357 PixHawk autopilot and Vaisala RSS421 sensors were logged at 5 Hz. Each logging event carried out by
358 the FlexLogger includes a sample time from the logger CPU clock, allowing for post-collection time
359 alignment between the different sensors. These sample times, along with artificial 5, 20, 50, 100, and 250
360 Hz clocks spanning the sample times between initial GPS lock and the last recorded sample time for the
361 VN-300, are used to align the different variables to a set of common clocks, primarily through one-
362 dimensional linear interpolation. One exception to the linear interpolation is the yaw estimate, which is
363 circular in nature (ranging between -180 and 180 degrees), and therefore uses a “nearest” interpolation to
364 ensure that the transition from 360 to 0 degrees is not represented as 180. During this interpolation
365 process, a limited number of points sharing a common sample time with another point are removed from
366 the record. Once these time variables are established, a *base_time* variable is established using the 250
367 Hz time stamp, and offsets from *base_time* are then calculated for all different logging resolutions.

368

369 The resampled (in time) dataset includes a variety of derived and measured quantities. Aircraft position,
370 including latitude, longitude, and altitude, are measured by the VN-300. The aircraft altitude is corrected
371 using a combination of various inputs from onboard GPS and pressure altimeters, as neither of these
372 altitude estimates can be used reliably as a definite flight altitude. Pressure altitude is subject to drift over
373 the duration of a single flight due to atmospheric evolution over a 2.5-hour window, potentially resulting
374 in values at landing that are higher or lower than those at take-off. Similarly, the accuracy of the GPS
375 altitude is insufficient to capture the vertical position of the aircraft to the level of detail required. To
376 calculate a true altitude, a combination of the autopilot altitude, VN-300 altitude, and VN-300 pressure
377 are used. First, a *flight_flag* variable is computed using airspeed and altitude information from the
378 autopilot. Any data points with airspeed exceeding 10 m s^{-1} and an altitude exceeding 5 m AGL is flagged

379 as a time when the aircraft is flying (*flight_flag=1*). The point at 200 samples (4 seconds) prior to the
380 first point in the record where the aircraft is deemed to be flying is recorded as the initial take-off index,
381 while the data point at 200 samples (4 seconds) after the last point in the record where the aircraft is
382 deemed to be flying is recorded as the landing index. The difference between the autopilot altitude at
383 these two indices is added into the flight record on a timestep-by-timestep basis, to correct for temporal
384 drift in pressure. A linear fit is then calculated to relate the VN-300 pressure and the difference between
385 the VN-300 reported altitude and the autopilot reported altitude. This pressure-dependent altitude
386 correction is then applied to the VN-300-reported altitude to derive a final altitude.

387

388 Wind estimation from fixed-wing aircraft requires the combination of several different measurements
389 related to airspeed, aircraft motion, and airflow over the aircraft (see van den Kroonenberg et al., 2008).
390 These measurements need to be of sufficient quality, and angular offsets and logging delays need to be
391 considered and removed. For RAAVEN, true airspeed (TAS) biases have a large impact on derivation of
392 wind speed, while the angular offsets between the MHP and INS and time-lag between the GPS and in
393 situ measurements have smaller impacts. These potential sources of error are corrected for using an
394 optimization technique, where small adjustments are made to the individual parameters and the
395 combination that results in the wind solution with the smallest overall variance is selected as the correct
396 winds.

397

398 For the RAAVEN WiscoDISCO-21 dataset, TAS is calculated using measurements from the MHP and
399 RSS421 probe using equation 1 from (Brown et al., 1983):

$$400 \quad TAS_i = \sqrt{\frac{2\bar{q}}{\rho}} \quad (1)$$

401 where ρ is the density of air calculated using the static pressure reported from the MHP, temperature from
402 the RSS421, and the specific gas constant for dry air, \bar{q} is defined as:

$$403 \quad \bar{q} = \frac{p_0}{1 - \frac{9}{4} \sin^2 \theta_a} \quad (2)$$

404 where $\sin^2 \theta_a$ is the total aerodynamic angle of the MHP, calculated using the angle of attack (α) and
405 sideslip angle (β) reported by the MHP.

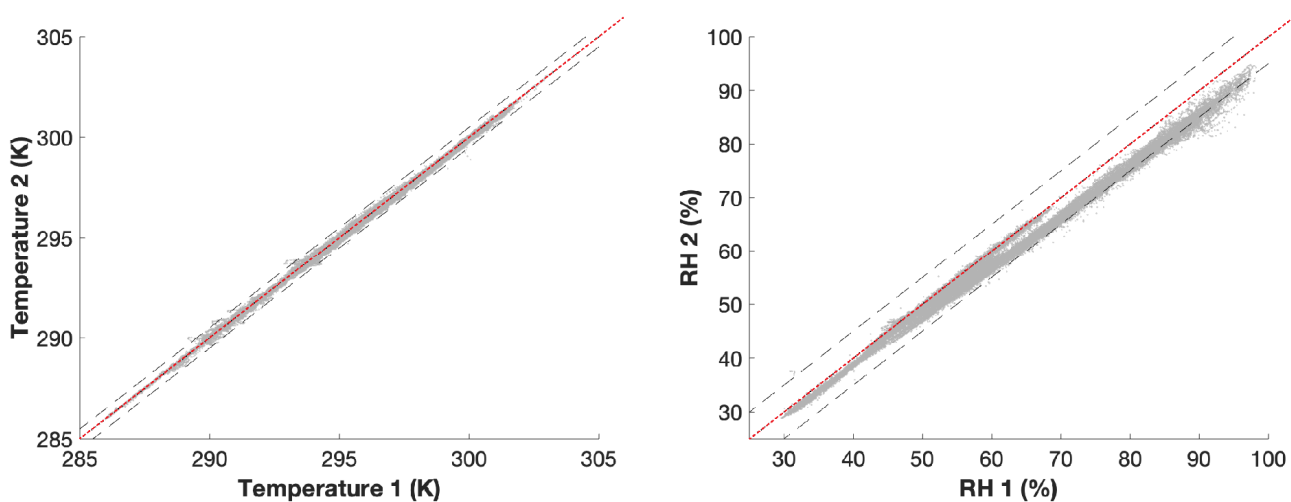
406

407 Based on testing in a temperature chamber, the pressure sensors used in this version of the MHP were
408 found to have non-linear temperature dependencies. This requires the application of an additional
409 temperature-dependent correction to ensure that an artificial alteration of TAS with altitude was not
410 present. Additional information on the calculation of airspeed and other quantities from the MHP can be
411 found in (de Boer et al., 2021a).

412

413 Derivation of the RAAVEN's thermodynamic measurements included multiple processing steps. First,
414 data from the two RSS421 sensors are averaged to attempt to reduce the influence of any solar exposure
415 of the sensors. Previous evaluations of the potential for solar contamination have not revealed any specific
416 biases on the observation (see de Boer et al., 2021a). Over the course of the WiscoDISCO-21 campaign,
417 the two sensors varied by less than 0.5 °C (Fig. 8). The averaged temperature time series was then used
418 to calibrate the coldwire data by applying a linear fit to the relationship between the coldwire voltage and
419 the temperature measured by the RSS421 sensor. The RSS421 relative humidity values were also
420 averaged. Typically, the RH measurements agreed to within 2%.

421



422

423 **Figure 8:** A comparison of temperature (left) and relative humidity (right) observations from the two
424 Vaisala RSS-421 sensors on RAAVEN for all flights. The red dotted lines represent a one-to-one
425 agreement, with the dashed black lines representing 0.5 degree (for temperature) and 5% (for relative
426 humidity) deviation from perfect agreement.

427

428 All quantities measured by the RAAVEN have data quality flags associated with them. For the RSS421-
429 derived temperature, the flag is set to zero for good data, and set to one for times when any of the following
430 occur: a) the absolute value of the difference between the temperature from either individual sensor and
431 the output temperature is greater than 0.5 °C, b) the absolute value of the difference between the output
432 temperature and the temperature from the EE-03 sensor on the MHP exceeds 5 °C, c) the recorded error
433 flag of either RSS421 sensor is active, or d) the aircraft is not flying. For the RH measurement from the
434 RSS421, a similar set of criteria are used to activate the data quality flag, except the limits are set to be
435 6% between RSS421 sensors, and 15% between the output RH value and the MHP-provided RH value.
436 The relative humidity values from the MHP are significantly impacted by the exposure of that sensor to
437 sunlight and the associated impact on sensor temperature. This is not corrected for, resulting in large
438 fluctuations in the RH values at times. As a result, this measurement (from the MHP) only provides a
439 reality check to ensure that the RSS421 are reporting accurate values, and therefore such a large offset
440 (15%) is allowed. The more important comparison is between the two RSS421 sensors, which should
441 agree much more closely, as they are the same sensor type, and are mounted within close proximity of
442 one another. The coldwire temperature data quality flag is activated when the difference between the
443 coldwire temperature and either of the RSS421 temperatures exceeds 1 °C, when the absolute value of
444 the difference between the coldwire temperature and the MHP temperature exceeds 3 °C, when the
445 coldwire voltage is observed to fall outside of the 0-4 V analog range, or when the aircraft is not flying.
446 Finally, the pressure quality control flag for the pressure measurement from the VN-300 is activated if
447 the absolute value of the difference between the reported VN-300 static pressure and that measured by
448 either of the RSS421 sensors exceeds 2.5 hPa. The RSS421 pressure measurements are not used because
449 they are believed to be biased low due to the airflow passing over their location on the aircraft.

450

451 In addition to the flags discussed above, we include a 3-stage flag for the wind measurements, which is
452 set to 0 (good data), 1 (suspect data) or 2 (bad data). Data are determined to be bad if any of the following
453 conditions were met:

- 454 - The measured angle of attack or sideslip exceeds 20 degrees, with values between 10-20
- 455 degrees are flagged as “suspect”
- 456 - The true airspeed (TAS) is below 10 m s⁻¹
- 457 - Any of the MHP ports are deemed to be blocked, as determined by the differential pressure
- 458 value for any of the sensors falling below -100 Pa
- 459 - The moving window variance of the MHP-derived TAS over 40 seconds is less than 5
- 460 - The aircraft is not flying
- 461 - The difference between the MHP TAS and that from the Pitot probe is greater than 5 m s⁻¹

462

463 Finally, we included two additional flags in the datastream to allow data users to better understand aircraft
464 flight state and support sampling during specific phases of flight. These flags include the “Flight_Flag”
465 introduced previously, as well as a “Flight_State” flag. The “Flight_State” flag includes information on
466 whether the is flying straight (0) or is turning (1) in the ones place, whether the aircraft is descending (0),
467 level (1), or ascending (2) in the tens place, and whether the aircraft is in flight (1) or not (0) in the
468 hundreds place. If, for example, a data user wanted to analyze straight, level flight legs, they would search
469 for data with “Flight_State” equal to 110. These flags are derived from information from a combination
470 of sensors, including the altitude variable described above, the aircraft yaw, and the “Flight_Flag” variable
471 described earlier on in this paragraph.

472

473 The accuracy of the RAAVEN observations has been evaluated in previous studies. For example, a
474 comparison of RAAVEN data with measurements collected by radiosondes launched from the Barbados
475 Cloud Observatory was conducted in recent work from de Boer et al., (2021b). While radiosondes in that
476 evaluation were launched approximately 20 km to the southeast, the air sampled by both systems was
477 largely representative of the marine boundary layer, implying limited spatial variability. In that
478 evaluation, the observations from the RAAVEN were very well correlated with those from the
479 radiosondes and do not show any positive or negative bias, supporting the idea that the RAAVEN
480 measurements provide an accurate depiction of the lower atmosphere. In addition, recent work allowed
481 for direct comparison of RAAVEN data to observations collected by radiosondes and a 60 m tower at the

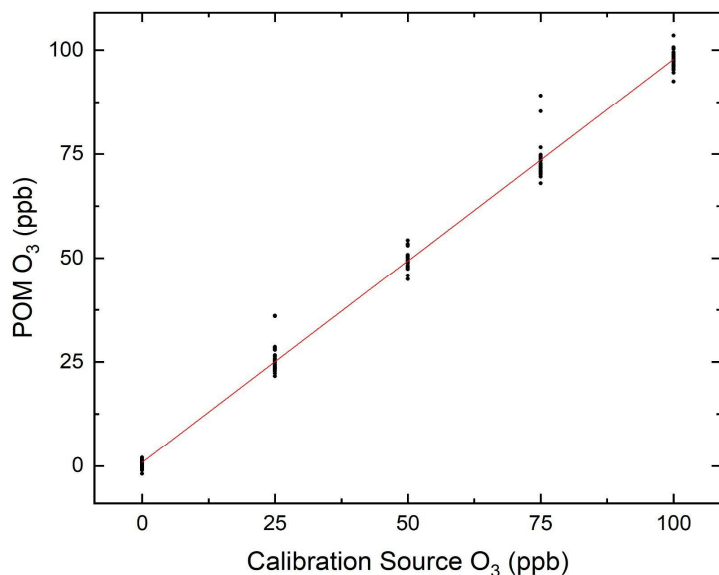
482 US Department of Energy's Southern Great Plains (SGP) research site. That study, de Boer et al. (2021a),
483 similarly provided confidence in the RAAVEN observations, showing close statistical agreement between
484 the different data sources.

485

486 **4.2 M210 UAS**

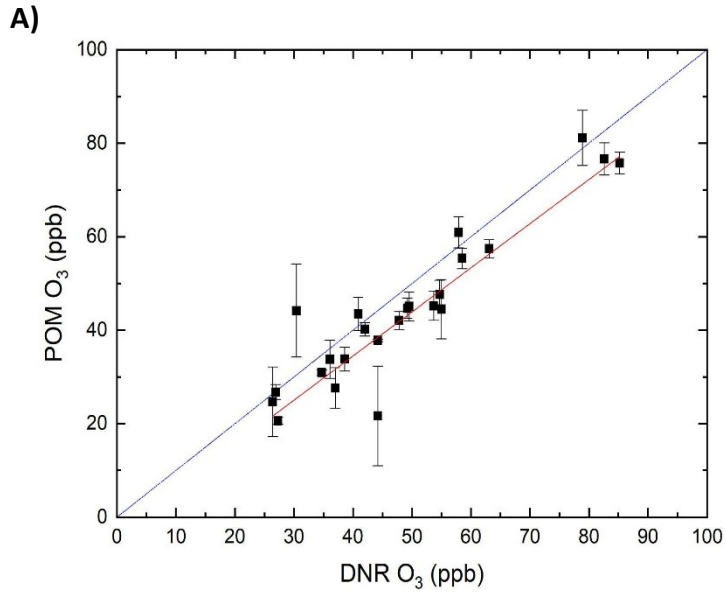
487 Data from the M210 flight controller, the POM and the iMET were all logged to individual instrument
488 internal data storage with independent timestamps. The average flight time of the M210 was 13.96 min.
489 The POM instrument logged data at 0.1 Hz. The iMET logged data every 10 Hz and the M210 flight log
490 recorded UAS GPS positioning and flight statistics at 100 Hz. The ozone concentrations from the POM
491 are adjusted to calibrated values, where ozone calibrations were conducted before every set of 2 flights
492 for the M210 using a 2BTech Model 306 ozone calibration source (Fig. 9). Data quality flags are
493 established as 0 = no concern, 1 = time flag, 2 = calibration and time flag. The time flag indicates flights
494 where the time offset between the M210 and the instrument time offset is large (iMET > 10 s or POM >
495 30 s). The calibration flag indicates when the POM was not responsive to the ozone calibration source
496 (Flight 5 on May 24) after an over-water flight. All times were averaged to 90 seconds and compressed
497 to the time window of observations for a single M210 ascent using the M210 timestamp. A time stamp
498 for 90s averaged data from all instrumentation on the M210 was generated by using the M210 timestamp
499 as primary and adjusting to a time offset in either the POM or the iMET for the start of a flight, then
500 averaged each variable for every 90 second interval of the flight. A 1σ standard deviation is presented as
501 the uncertainty for the 90-s averages. The iMET observations of temperature, relative humidity, pressure
502 and humidity temperature are presented using the 90-s averages with uncertainty as 1σ standard
503 deviations. Each flight ascent start and end were determined by observed changes in atmospheric pressure
504 by the iMET sensor, altitude change in the M210, or noted time of ascent in field notebook for the POM.
505 The altitudes for each observation were obtained by averaging the M210 flight log altitude data for the
506 90-s timestamps. The flight data timestamps varied slightly for each data source. The POM time drift was
507 the most pronounced, with an average difference between the iMet of ~ 24 s. The POM's time was
508 adjusted manually throughout the campaign as the time would drift over the course of one flight. The
509 average difference between the iMet and the M210 over 20 flights was ~ 4 s. Only 20% of flights had a

510 time-difference between iMET and M210 greater than 10 seconds. Instrument battery loss occurred for
511 the iMET system which resulted in lost data for a 2flights on May 26, 2021.



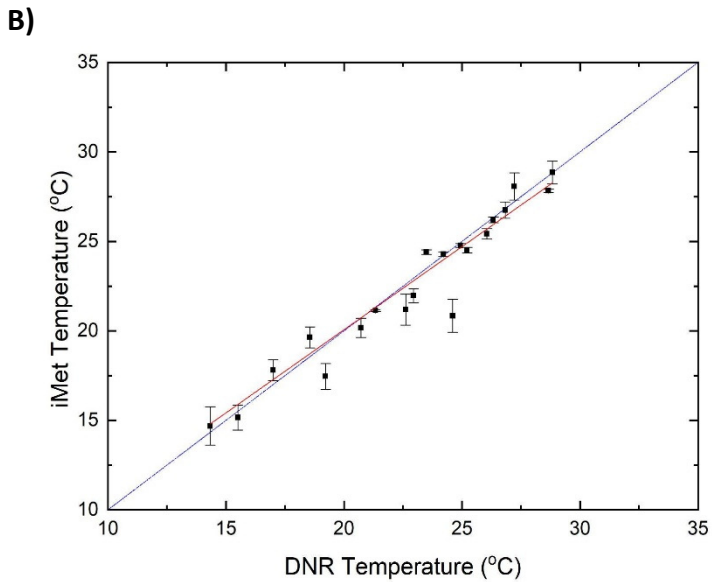
512 **Figure 9:** A sample POM calibration from May 24, 2021. The linear regression fit gives: $y = 0.9689 (\pm$
513 $0.0061) x + 0.83 (\pm 0.35)$, $R^2 = 0.9937$. Each calibration concentration had a 5-minute duration with the
514 POM logging 10-s data.
515
516

517 Intercomparison between observations made via instrumentation on the M210 at 5 m AGL and at the Wi-
518 DNR ground station show a linear agreement between the observations (Fig. 10). The linear agreement is
519 better for the iMET temperature and the ground station temperature with $R^2 = 0.970$ in comparison to R^2
520 $= 0.955$ for O₃ observations. The O₃ linear fit, $O_3 (\text{POM}) = 0.944 (\pm 0.044) O_3 (\text{DNR}) - 3.3 (\pm 1.9)$, has a
521 negative intercept. The uncertainties in the POM's O₃ concentrations are much larger than uncertainties
522 in the ground station instrumentation. The linear agreement between the different instrumentation on
523 separate observation platforms demonstrates that the M210 platform instrumentation provides an
524 accurate, albeit less precise representation of the atmosphere.
525



545

544



562 **Figure 10:** Intercomparison between measurements from instrumentation on the M210 at 5 m AGL and
 563 at the WI-DNR ground station for a) O₃ (ppb) observations and b) temperature (° C). Blue lines depict
 564 1:1 agreement and red lines depict the linear regression best fit with a) $O_{3(POM)} = 0.944 (\pm 0.044) O_{3(DNR)} - 3.3 (\pm 1.9)$, $R^2 = 0.955$, and b) $T_{iMET} = 0.929 (\pm 0.038) T_{DNR} + 1.48 (\pm 0.93)$, $R^2 = 0.970$.
 565
 566

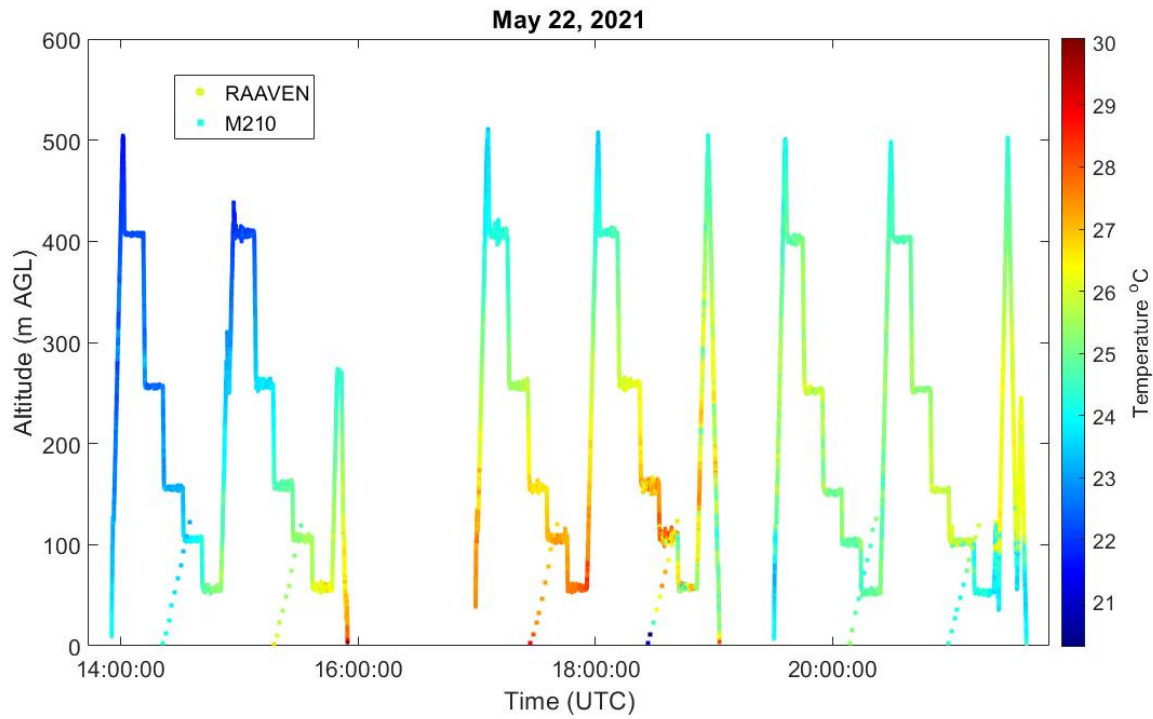
567 **5. Data Availability and File Structure**

568 A community data repository has been established for this field campaign at
569 <https://zenodo.org/communities/wiscodisco21/>. The data sets in the repository cover the merged iMET
570 and POM data sets from the M210 (DOI:10.5281/zenodo.5160346) as .txt files, the RAAVEN dataset
571 (DOI: 10.5281/zenodo.5142491) as .cdf files, and the doppler lidar wind profiler (DOI:
572 10.5281/zenodo.5213039) as .cdf files. M210 files have a naming convention that includes
573 WiscoDisco_M210_YYYYMMDD_F#, where the flight number for the day is indicated by F#. RAAVEN
574 files have a naming convention that includes WiscoDisco_CU-
575 RAAVEN_YYYYMMDD_hhmmss_B1.nc, where YYYYMMDD is the year, month and day that the
576 data were collected, hhmmss is the time of power on for the aircraft, and B1 is the data processing level,
577 where B1 files have had data quality checks and post-processing (e.g. coldwire calibration and wind
578 estimation) applied. The Doppler lidar files have a naming convention that includes
579 chiwaukee_wind_profiles_YYYYMMDD and chiwaukee_stare_YYYYMMDD. All datasets include geospatial
580 information (latitude, longitude, altitude) and timestamps in UTC.

581 **6. Interpreted Results**

582 The WiscoDISCO-21 project demonstrates how UAS can be used to sample a complex circulation
583 near to the surface without causing major disruption to people, wildlife and ecosystems in the area. An
584 example of a characterization of lake breeze incursion is shown in Figures 11 and 12, which include the
585 temperature profiles from the M210 and RAAVEN (Fig. 11) and Doppler lidar u wind component (Fig.
586 12). The temperature profiles from the M210 and RAAVEN show a notable temperature inversion in the
587 late afternoon below 150 m and the Doppler lidar u wind component shows easterly winds arriving after
588 18:00 UTC. The combination of u component winds from Doppler lidar and the temperature observations
589 from the UAS platforms are consistent in demonstrating a marine layer incursion with maximum height
590 of approximately 250 m AGL at 21:00 UCT collapsing to a height of 100 m AGL by 22:00 UTC. The
591 nonuniform start to the lake breeze onset fluctuated, shown as shifting u component winds from easterly
592 to westerly after 18:00 UTC (Fig. 12) and disagreement with the lowest altitude observations from the
593 M210 and RAAVEN between 18:30-19:00 UTC (Fig. 11). The distance between the M210 launch site

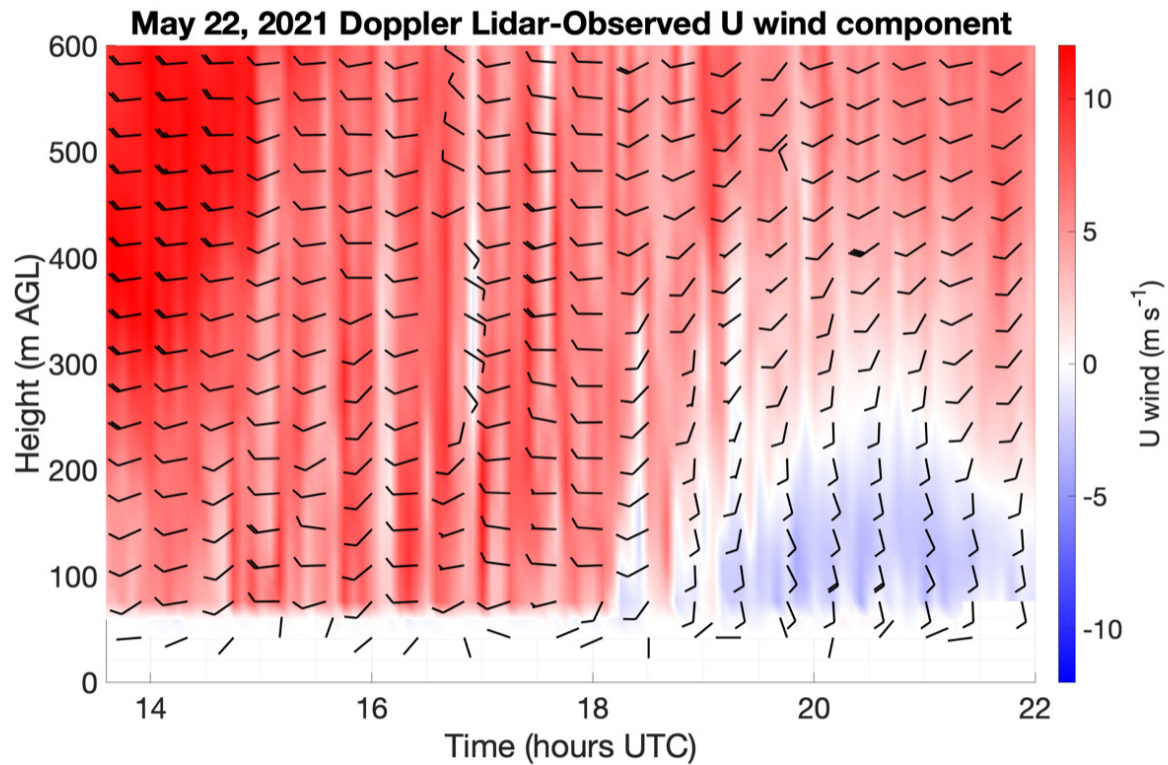
594 and the RAAVEN landing site complicates the low altitude observations of temperatures between 18:00
595 and 19:00 UTC, which also may indicate the very limited incursion of the lake breeze at that time.



596

597

598 **Figure 11:** Temperatures ($^{\circ}$ C) measured from University of Colorado RAAVEN (O) and the M120 (\square)
599 on May 22, 2021. RAAVEN was flying over-prairie circular spirals Pattern A.



600

601 **Figure 12:** Time/height cross section of the u (zonal) component of the Doppler lidar-observed
 602 horizontal winds (in m/s), overlaid with horizontal wind barbs (in kts) plotted according to the standard
 603 convention from May 22, 2021. Wind barbs are thinned by a factor of five in the time dimension and a
 604 factor of two in the height dimension to aid readability.

605 **7. Summary**

606

607 The 2021 WiscoDISCO field campaign incorporated the use of two UAS platforms for meteorological
 608 and chemical measurements in the atmosphere, a multirotor completing vertical profiles up to 120 m AGL
 609 and a fixed wing executing flight patterns up to 500 m AGL alongside a Lidar WindPro instrument
 610 capable of sensing winds and aerosol backscatter from altitudes of 100-2000 m AGL. The overlapping
 611 domains are useful for characterizing low altitude mesoscale meteorology of the lake breeze at a shoreline
 612 environment that regularly observes ozone enhancement events during onshore flow. Data from all
 613 instruments and platforms have been compiled, quality-control tested and uploaded to a community
 614 repository. The collaborative field campaign involved teams from 4 different universities and obtained

615 continuous lidar data in conjunction with 24 flight hours of fixed wing and 6 flight hours of multi-rotor
616 vertical profiles on days likely impacted by lake breeze.

617

618 The data from the WiscoDISCO-21 campaign can be used to evaluate the markers for lake breeze
619 incursion overland in winds, temperatures, chemical composition and optical properties (backscatter).
620 The thermodynamic conditions for lake breeze incursion at a local scale can be determined through the
621 evaluation of horizontal and vertical winds, atmospheric stability and potential temperature. The
622 positioning of pollutants with respect to the marine layer markers can also be investigated.

623

624 **Author Contributions.**

625 Patricia A. Cleary is the PI of this project and was responsible for data collection, overseeing data analysis
626 from the M210, field campaign planning and logistics, and the writing and editing of this document. Ben
627 Kies was responsible for data collection for the M210 in the field, Joe Tirado was responsible for data
628 analysis, quality control and data formatting for the repository for the M210, Aidan Voon was responsible
629 for data analysis for the M210. Joe Hupy was responsible for piloting the M210 and the writing and
630 editing of this paper. Gijs de Boer was responsible for coordination and execution of the University of
631 Colorado RAAVEN flights, and for development, writing and editing of the publication. Steve Borenstein
632 and Jonathan Hamilton contributed to the collection of the RAAVEN dataset as field operators, and
633 supported the development of this manuscript. Dale Lawrence supplied instrumentation for the RAAVEN
634 UAS and contributed to the writing of the manuscript. Tim Wagner and R Bradley Pierce were
635 responsible for data collection, data analysis of the doppler lidar instrumentation, and writing and editing
636 this document and R Bradley Pierce assisted in field planning.

637

638

639 **Competing Interests.**

640 GB works as a consultant for Black Swift Technologies, who manufacture the multi-hole pressure probe
641 used in the collection of the RAAVEN dataset.

642

643

644 **Acknowledgements.**

645 This material is based upon work funded by the National Science Foundation award #1918850. The UW-
646 Eau Claire team acknowledges support from the Student Blugold Commitment Differential Tuition
647 program. The University of Colorado team acknowledges financial support from the University of
648 Wisconsin Eau-Claire through a sub-contract supported by the US National Science Foundation, as well
649 as support from the NOAA Physical Sciences Laboratory. Any opinions, findings, and conclusions or
650 recommendations expressed in this material are those of the author(s) and do not necessarily reflect the
651 views of the National Science Foundation. The authors thank Nathan Taminger and Paul McKinley for
652 their participation in the WiscDISCO-21 field campaign.

653

654 **References**

655

- 656 Abdi-Oskouei, M., Carmichael, G., Christiansen, M., Ferrada, G., Roozitalab, B., Sobhani, N., Wade,
657 K., Czarnetzki, A., Pierce, R. B., Wagner, T., and Stanier, C.: Sensitivity of Meteorological Skill to
658 Selection of WRF-Chem Physical Parameterizations and Impact on Ozone Prediction During the Lake
659 Michigan Ozone Study (LMOS), *Journal of Geophysical Research-Atmospheres*, 125, 25,
660 10.1029/2019jd031971, 2020.
- 661 Brown, E. N., Friehe, C. A., and Lenschow, D. H.: THE USE OF PRESSURE-FLUCTUATIONS ON
662 THE NOSE OF AN AIRCRAFT FOR MEASURING AIR MOTION, *Journal of Climate and Applied
663 Meteorology*, 22, 171-180, 10.1175/1520-0450(1983)022<0171:Tuopfo>2.0.Co;2, 1983.
- 664 Caicedo, V., Delgado, R., Luke, W. T., Ren, X. R., Kelley, P., Stratton, P. R., Dickerson, R. R.,
665 Berkoff, T. A., and Gronoff, G.: Observations of bay-breeze and ozone events over a marine site during
666 the OWLETS-2 campaign, *Atmospheric Environment*, 263, 10.1016/j.atmosenv.2021.118669, 2021.
- 667 Cleary, P. A., Fuhrman, N., Schulz, L., Schafer, J., Fillingham, J., Bootsma, H., McQueen, J., Tang, Y.,
668 Langel, T., McKeen, S., Williams, E. J., and Brown, S. S.: Ozone distributions over southern Lake
669 Michigan: comparisons between ferry-based observations, shoreline-based DOAS observations and
670 model forecasts, *Atmospheric Chemistry and Physics*, 15, 5109-5122, 10.5194/acp-15-5109-2015,
671 2015.
- 672 Cleary, P. A., Dickens, A. J., McIlquham, M., Sanchez, M., Geib, K., Hedberg, C., Hupy, J., Watson,
673 M. W., Fuoco, M., Olson, E. R., Pierce, R. B., Stanier, C., Long, R., Valin, L., Conley, S., and Smith,
674 M.: Impacts of lake breeze meteorology on ozone gradient observations along Lake Michigan
675 Shorelines in Wisconsin: 2017 LMOS examples in press, *Atmospheric Environment*, 2022.
- 676 de Boer, G., Borenstein, S., Hamilton, J., Osborn, J., Lawrence, D., Argrow, B., and Intrieri, J.:
677 Measurements from the University of Colorado RAAVEN Uncrewed Aircraft System during ATOMIC,
678 *Earth System Science Data*, submitted, 2021a.
- 679 de Boer, G., Elston, J., Houston, A., Pillar-Little, E., Argrow, B., Bell, T., Chilson, P., Choate, C.,
680 Greene, B., Islam, A., Detweiler, C., Jacob, J., Natalie, V., Rhodes, M., Rico, D., Stachura, M., Lappin,
681 F., Whyte, S., and Wilson, M.: Evaluation and Intercomparison of Small Uncrewed Aircraft Systems

682 Used for Atmospheric Research, in preparation, *Journal of Atmospheric and Oceanic Technology*,
683 2021b.

684 Doak, A. G., Christiansen, M. B., Alwe, H. D., Bertram, T. H., Carmichael, G., Cleary, P., Czarnetzki,
685 A. C., Dickens, A. F., Janssen, M., Kenski, D., Millet, D. B., Novak, G. A., Pierce, B. R., Stone, E. A.,
686 Long, R. W., Vermeuel, M. P., Wagner, T. J., Valin, L., and Stanier, C. O.: Characterization of ground-
687 based atmospheric pollution and meteorology sampling stations during the Lake Michigan Ozone Study
688 2017, *Journal of the Air & Waste Management Association*, 71, 866-889,
689 10.1080/10962247.2021.1900000, 2021.

690 Dye, T. S., Roberts, P. T., and Korc, M. E.: Observations of transport processes for ozone and ozone
691 precursors during the 1991 Lake Michigan Ozone Study, *Journal of Applied Meteorology*, 34, 1877-
692 1889, 10.1175/1520-0450(1995)034<1877:ootpfo>2.0.co;2, 1995.

693 Elston, J., Argrow, B., Stachura, M., Weibel, D., Lawrence, D., and Pope, D.: Overview of Small Fixed-
694 Wing Unmanned Aircraft for Meteorological Sampling, *Journal of Atmospheric and Oceanic*
695 *Technology*, 32, 97-115, 10.1175/jtech-d-13-00236.1, 2015.

696 Foley, T., Betterton, E. A., Jacko, P. E. R., and Hillery, J.: Lake Michigan air quality: The 1994-2003
697 LADCO Aircraft Project (LAP), *Atmospheric Environment*, 45, 3192-3202,
698 10.1016/j.atmosenv.2011.02.033, 2011.

699 Frew, E. W., Argrow, B., Borenstein, S., Swenson, S., Hirst, C. A., Havenga, H., and Houston, A.: Field
700 observation of tornadic supercells by multiple autonomous fixed-wing unmanned aircraft, *Journal of*
701 *Field Robotics*, 37, 1077-1093, 10.1002/rob.21947, 2020.

702 Geddes, J. A., Wang, B., and Li, D.: Ozone and Nitrogen Dioxide Pollution in a Coastal Urban
703 Environment: The Role of Sea Breezes, and Implications of Their Representation for Remote Sensing
704 of Local Air Quality, *Journal of Geophysical Research-Atmospheres*, 126, 10.1029/2021jd035314,
705 2021.

706 Gronoff, G., Robinson, J., Berkoff, T., Swap, R., Farris, B., Schroeder, J., Halliday, H. S., Knepp, T.,
707 Spinei, E., Carrion, W., Adcock, E. E., Johns, Z., Allen, D., and Pippin, M.: A method for quantifying
708 near range point source induced O-3 titration events using Co-located Lidar and Pandora measurements,
709 *Atmospheric Environment*, 204, 43-52, 10.1016/j.atmosenv.2019.01.052, 2019.

710 Guimaras, P., Ye, J. H., Batista, C., Barbosa, R., Ribeiro, I., Medeiros, A., Zhao, T. N., Hwang, W. C.,
711 Hung, H. M., Souza, R., and Martin, S. T.: Vertical Profiles of Atmospheric Species Concentrations and
712 Nighttime Boundary Layer Structure in the Dry Season over an Urban Environment in Central Amazon
713 Collected by an Unmanned Aerial Vehicle, *Atmosphere*, 11, 10.3390/atmos11121371, 2020.

714 Hayden, K. L., Sills, D. M. L., Brook, J. R., Li, S. M., Makar, P. A., Markovic, M. Z., Liu, P., Anlauf,
715 K. G., O'Brien, J. M., Li, Q., and McLaren, R.: Aircraft study of the impact of lake-breeze circulations
716 on trace gases and particles during BAQS-Met 2007, *Atmospheric Chemistry and Physics*, 11, 10173-
717 10192, 10.5194/acp-11-10173-2011, 2011.

718 Holton, J.: *An Introduction to Dynamic Meteorology*, third ed., Academic Press, San Diego 1992.

719 Horel, J., Crosman, E., Jacques, A., Blaylock, B., Arens, S., Long, A., Sohl, J., and Martin, R.: Summer
720 ozone concentrations in the vicinity of the Great Salt Lake, *Atmospheric Science Letters*, 17, 480-486,
721 10.1002/asl.680, 2016.

722 Jozef, G., Cassano, J., Dahlke, S., and de Boer, G.: Testing the efficacy of boundary layer height
723 detection algorithms using uncrewed aircraft system data from MOSAIC, *Atmos. Meas. Tech.*,
724 submitted.

725 Keen, C. S. and Lyons, W. A.: Lake/Land Breeze circulations on the western shore of Lake Michigan,
726 *Journal of Applied Meteorology*, 17, 1843-1855, 10.1175/1520-0450(1978)017<1843:lbcotw>2.0.co;2,
727 1978.

728 Lennartson, G. J. and Schwartz, M. D.: The lake breeze-ground-level ozone connection in eastern
729 Wisconsin: A climatological perspective, *International Journal of Climatology*, 22, 1347-1364,
730 10.1002/joc.802, 2002.

731 Levy, I., Makar, P. A., Sills, D., Zhang, J., Hayden, K. L., Mihele, C., Narayan, J., Moran, M. D.,
732 Sjostedt, S., and Brook, J.: Unraveling the complex local-scale flows influencing ozone patterns in the
733 southern Great Lakes of North America, *Atmospheric Chemistry and Physics*, 10, 10895-10915,
734 10.5194/acp-10-10895-2010, 2010.

735 Lyons, W. A. and Cole, H. S.: Photochemical oxidant transport - Mesoscale lake breeze and synoptic-
736 scale aspects, *Journal of Applied Meteorology*, 15, 733-743, 10.1175/1520-
737 0450(1976)015<0733:potmlb>2.0.co;2, 1976.

738 Lyons, W. A. and Olsson, L. E.: Detailed mesometeorological studies of air pollution dispersion in
739 Chicago lake breeze, *Monthly Weather Review*, 101, 387-403, 10.1175/1520-
740 0493(1973)101<0387:dmsop>2.3.co;2, 1973.

741 Martin, J. E.: *Mid-Latitude Atmospheric Dynamics: A First Course*, John Wiley & Sons, West
742 Sussex 2006.

743 McNider, R. T., Pour-Biazar, A., Doty, K., White, A., Wu, Y. L., Qin, M. M., Hu, Y. T., Odman, T.,
744 Cleary, P., Knipping, E., Dornblaser, B., Lee, P., Hain, C., and McKeen, S.: Examination of the
745 Physical Atmosphere in the Great Lakes Region and Its Potential Impact on Air Quality Overwater
746 Stability and Satellite Assimilation, *Journal of Applied Meteorology and Climatology*, 57, 2789-2816,
747 10.1175/jamc-d-17-0355.1, 2018.

748 Miller, S. T. K., Keim, B. D., Talbot, R. W., and Mao, H.: Sea breeze: Structure, forecasting, and
749 impacts, *Reviews of Geophysics*, 41, 10.1029/2003rg000124, 2003.

750 Qin, M. M., Yu, H. F., Hu, Y. T., Russell, A. G., Odman, M. T., Doty, K., Pour-Biazar, A., McNider, R.
751 T., and Knipping, E.: Improving ozone simulations in the Great Lakes Region: The role of emissions,
752 chemistry, and dry deposition, *Atmospheric Environment*, 202, 167-179,
753 10.1016/j.atmosenv.2019.01.025, 2019.

754 Sills, D. M. L., Brook, J. R., Levy, I., Makar, P. A., Zhang, J., and Taylor, P. A.: Lake breezes in the
755 southern Great Lakes region and their influence during BAQS-Met 2007, *Atmospheric Chemistry and*
756 *Physics*, 11, 7955-7973, 10.5194/acp-11-7955-2011, 2011.

757 Stanier, C. O., Pierce, R. B., Abdi-Oskouei, M., Adelman, Z. E., Al-Saadi, J., Alwe, H. D., Bertram, T.
758 H., Carmichael, G. R., Christiansen, M. B., Cleary, P. A., Czarnetzki, A. C., Dickens, A. F., Fuoco, M.
759 A., Hughes, D. D., Hupy, J. P., Janz, S. J., Judd, L. M., Kenski, D., Kowalewski, M. G., Long, R. W.,
760 Millet, D. B., Novak, G., Roozitalab, B., Shaw, S. L., Stone, E. A., Szykman, J., Valin, L., Vermeuel,
761 M., Wagner, T. J., and Whitehill, A. R.: Overview of the Lake Michigan Ozone Study 2017, *Bulletin of*
762 *the American Meteorological Society*, doi.org/10.1175/BAMS-D-20-0061.1, 2021.

763 Vermeuel, M. P., Novak, G. A., Alwe, H. D., Hughes, D. D., Kaleel, R., Dickens, A. F., Kenski, D.,
764 Czarnetzki, A. C., Stone, E. A., Stanier, C. O., Pierce, R. B., Millet, D. B., and Bertram, T. H.:
765 Sensitivity of Ozone Production to NO_x and VOC Along the Lake Michigan Coastline, *Journal of*
766 *Geophysical Research-Atmospheres*, 124, 10989-11006, 10.1029/2019jd030842, 2019.
767 Wagner, T. J., Klein, P. M., and Turner, D. D.: A NEW GENERATION OF GROUND-BASED
768 MOBILE PLATFORMS FOR ACTIVE AND PASSIVE PROFILING OF THE BOUNDARY LAYER,
769 *Bulletin of the American Meteorological Society*, 100, 137-153, 10.1175/bams-d-17-0165.1, 2019.
770 Wagner, T. J., Czarnetzki, A. C., Christiansen, M., Pierce, R. B., Stanier, C. O., Dickens, A. F., and
771 Eloranta, E. W.: Observations of the Development and Vertical Structure of the Lake Breeze
772 Circulation During the 2017 Lake Michigan Ozone Study, Submitted, 2021.
773 Wagner, T. J., Czarnetzki, A. C., Christiansen, M., Pierce, R. B., Stanier, C. O., Dickens, A. F., and
774 Eloranta, E. W.: Observations of the Development and Vertical Structure of the Lake Breeze
775 Circulation During the 2017 Lake Michigan Ozone Study, *Journal of the Atmospheric Sciences*,
776 <https://doi.org/10.1175/JAS-D-20-0297.1>, 2022.
777 Wentworth, G. R., Murphy, J. G., and Sills, D. M. L.: Impact of lake breezes on ozone and nitrogen
778 oxides in the Greater Toronto Area, *Atmospheric Environment*, 109, 52-60,
779 10.1016/j.atmosenv.2015.03.002, 2015.
780 Wildmann, N., Ravi, S., and Bange, J.: Towards higher accuracy and better frequency response with
781 standard multi-hole probes in turbulence measurement with remotely piloted aircraft (RPA),
782 *Atmospheric Measurement Techniques*, 7, 1027-1041, 10.5194/amt-7-1027-2014, 2014.
783